

A Heterogeneous Constitutive Model for Reinforced Carbon-Carbon using LS-DYNA[®]

Kelly S. Carney, Robert K. Goldberg, J. Michael Pereira
NASA Glenn Research Center, 21000 Brookpark Rd., Cleveland, Ohio, 44135, USA

Ryan S. Lee, Jeremie J. Albert
The Boeing Company, Rotorcraft Division, Structures, Technology, and Prototyping,
Industrial Hwy and Stewart Ave., Ridley Park, PA 19078, USA

Abstract

Reinforced Carbon-Carbon (RCC) is a ceramic matrix, coated C/C composite used in the Space Shuttle's thermal protection system. A constitutive model for RCC is presented that separates the coating and substrate within a multi-material shell element allowing for bending strains to be accurately computed during a finite element analysis. Version 971 of LS-DYNA contains a new shell element formulation that allows for different constitutive models through the thickness. The carbon substrate is modeled with an orthotropic damage model that was originally developed by Matzenmiller, and has been enhanced into MAT_RATE_SENSITIVE_COMPOSITE_FABRIC (MAT 158). The behavior of the silicon carbide coating is modeled using a new constitutive model that is now included in LS-DYNA as MAT_NONLINEAR_ELASTIC_TENSION_CRACKS (MAT 236). The composite model is used for debris impact analysis on the RCC structures, and good correlation is shown with impact test deflections and damage.

Introduction

The Space Shuttle Orbiter is highly dependent on its thermal protection systems (TPS) that allow the vehicle to re-enter the atmosphere under intense aerodynamic heating. The TPS is comprised of thermal blankets, tiles, and for the hottest regions, a material known as Reinforced Carbon-Carbon, or RCC. The Orbiter's wing leading edges (WLE) are constructed with 22 RCC panels on each wing (Figure 1) and the somewhat larger RCC Nose Cap, along with RCC "T" seals that cover the gaps between panels (1). The primary function of the panels are to provide an aerodynamic surface that can withstand the intense heat of an atmospheric re-entry cycle, which can yield temperatures in excess of 2000° F for several minutes. The panels must also withstand the debris environment, which can potentially include foam, ice, and other TPS materials, reaching speeds of up to 2500 ft/sec, resulting in severe impact conditions from even low-density debris such as insulating foam.

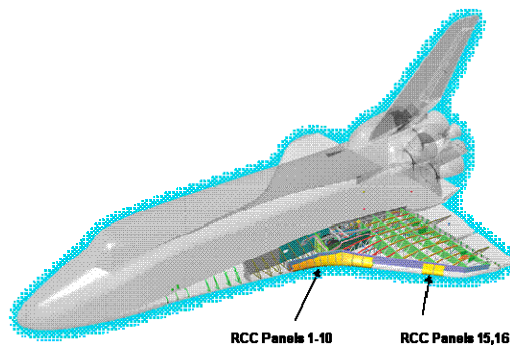


Figure 1. RCC Panels on the orbiter wing leading edge (2).

In February 2003, the Space Shuttle Orbiter *Columbia* disintegrated while re-entering the atmosphere, killing all seven astronauts aboard mission STS-107. One of the recommendations of the Columbia Accident Investigation Board (CAIB) (2) was to develop a methodology to understand and predict the capability of the RCC WLE and Nose Cap to withstand various ascent debris impacts. Since RCC panels cost in excess of \$1 million each, finite element analysis, verified by testing, would have to be used to determine RCC capability. The testing program would adopt a “ground-up” approach: RCC mechanical property tests would be used for constitutive model development, followed by many small-scale impact tests on flat plates (3), and finishing up with a very few number of full-scale panel impact tests (4) to validate the analytical model.

To perform the analysis, the Orbiter Program utilized the commercially available explicit, finite-element analysis code LS-DYNA (5) and formed a NASA/Boeing team to develop a RCC specific methodology to re-certify the Shuttle for flight (6). With this new tool and the understanding gained of RCC impact resistance has flown multiple successful missions since the Columbia accident in 2003. However, due to time constraints and then current technical limitations, the NASA/Boeing team assumed that the RCC was a smeared property, homogeneous material with uniform material properties at all points throughout the material thickness (7). The RCC material is actually composed of a woven carbon/carbon substrate with a silicon carbide outer coating. In the improved approach described in this article, the substrate and coating are modeled separately. By separating the representation of the substrate and the coating, an accurate stress distribution through an element is possible, variations of the coating thickness can be accounted for, and the damage and failure of the material can be more explicitly represented.

RCC Overview

Reinforced Carbon-Carbon, or RCC, is a woven carbon fiber composite with a 0°/90° weave, at least 19 layers, and a ceramic carbon matrix. Two plies on the inner and outer surfaces consist of silicon carbide. The entire laminate, both carbon substrate and silicon carbide coating, is highly non-uniform, as can be seen in the cross-sectional views in Figure 2. The coating is neither pure silicon carbide, nor can it be made in a way such that it is independent of the carbon substrate. Because of this, detailed testing of the bulk coating material is not possible. Non-uniform cracks (referred to as “craze-cracks”) also exist in the coating which make its properties very different from that of bulk SiC.

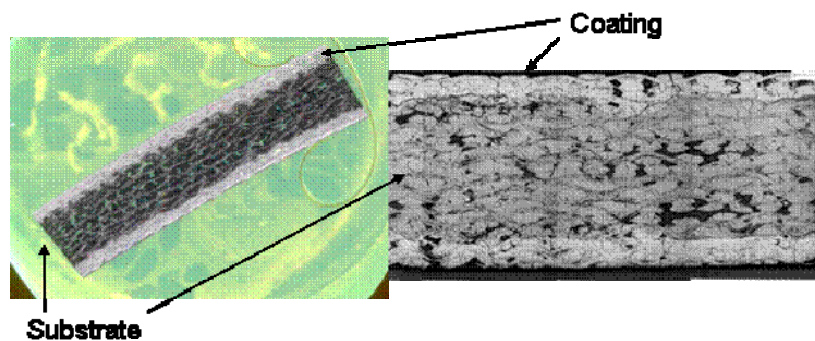


Figure 2. Cross-sectional views of RCC laminate.

Figure 3 shows that the RCC laminate material properties has large, significant scatter (8). Note the large difference between the tension and compression properties and the significant non-linear deformation response. All of these features need to be accounted for within the constitutive model of the material. Also note that all of the stress-strain plots in this paper are normalized to the average substrate failure stress and strain.

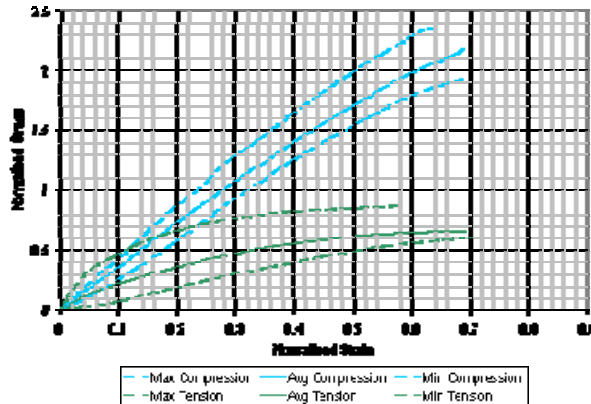


Figure 3. Normalized as-fabricated RCC tension and compression stress strain response.

Material tests were also performed with the un-coated, carbon-carbon substrate only. By using this data and the rule of mixtures, as was performed by Baccus (9), it is possible to predict what the properties of the silicon carbide coating. The thicknesses of these layers are approximately known, and are labeled in Figure 4 as t_{SiC} and t_{sub} respectively. The stress in each layer is σ_{SiC} (unknown) and σ_{sub} (known from substrate tests), and the overall laminate stress (known from laminate tests) is σ_{lam} . The rule of mixtures states that the overall laminate stress will be given by

$$\sigma_{lam} \cdot t_{lam} = \sigma_{sub} \cdot t_{sub} + \sigma_{SiC} \cdot t_{SiC} , \tag{1}$$

with the only unknown being the coating stress. In this manner, the rule of mixtures yields the macroscopic coating properties for as-fabricated RCC.

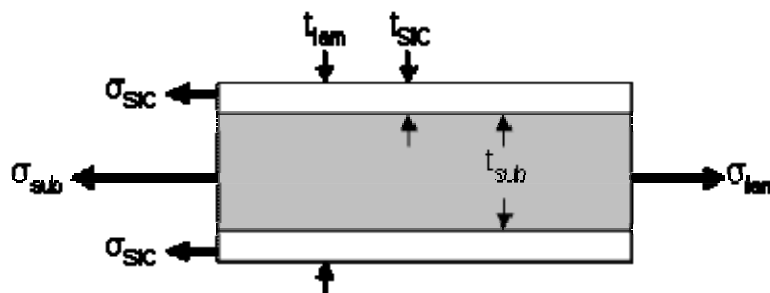


Figure 4. An idealized RCC cross-section.

The measured RCC laminate and the predicted constituent properties for in-plane tension and compression are presented in Figures 5 and 6. Note that in tension, the coating will only take a small amount of load in comparison to the substrate before quickly degrading. This behavior is consistent with the response typically observed in ceramic matrix composites. In compression, the coating is stiffer than the substrate and nearly linear.

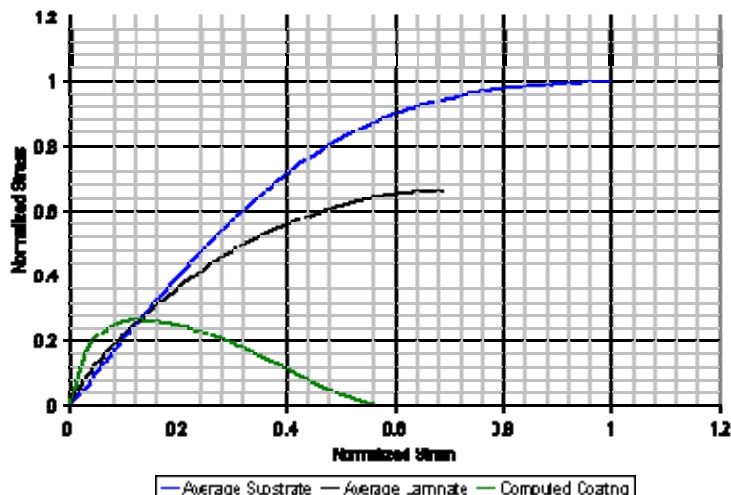


Figure 5. Average laminate and substrate tension response, with computed coating response in tension.

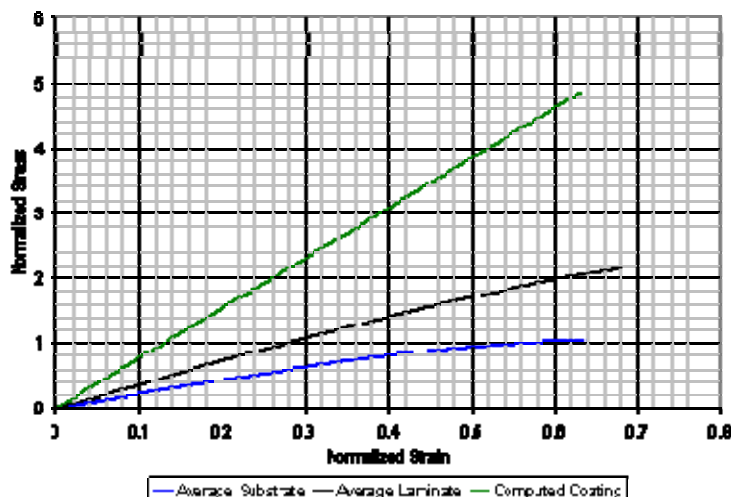


Figure 6. Average laminate and substrate compression response, with computed coating response in compression.

Based on the limited shear strain results, it appears that the coating shares some of the carbon fabric’s orthotropy; the non-homogeneity of the coating is visible in the RCC specimen in Figure 7.

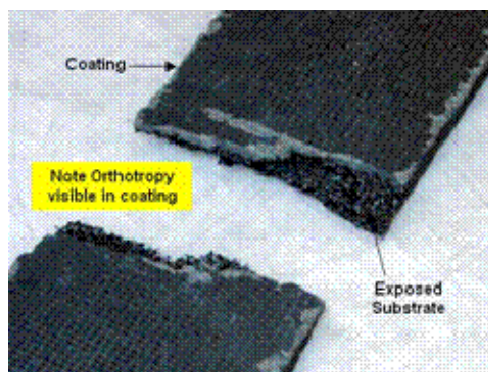
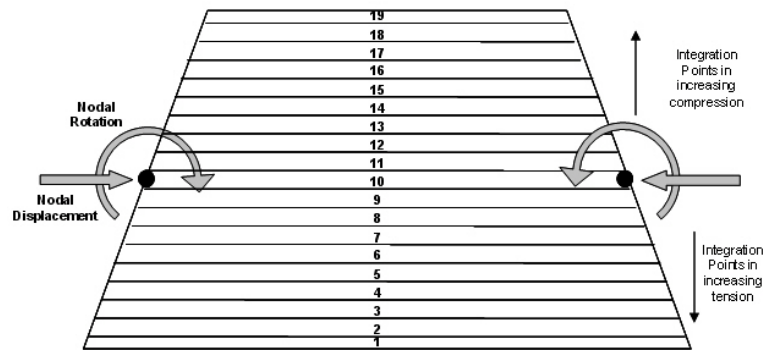


Figure 7. A split RCC specimen with orthotropy visible in coating.

Heterogeneous RCC Model

Multi-Material Shell

Version 971 of LS-DYNA contains a new shell element formulation that allows for different constitutive models through the thickness (10). The end result is a single shell element that is numerically equivalent to many shells stacked together and tied at the nodes such that there is a rigid, rotating constraint through the thickness. A nodal displacement and rotational consistency condition exists to capture bending within the element (Figure 8). These consistency conditions constrain the displacements of each layer, however the differing constitutive models result in varying stresses through the thickness.



Nodal displacements and rotations are converted into integration point strains. Thus, bending is not computed at each integration point; only in-plane response is computed. By having a full 19 integration points, and two for each coating layer, the laminate bending response is captured. LS-DYNA computes the updated nodal force and moments at each timestep based on the stresses at each integration point.

Figure 8. Multi-layer shell element in bending.

When using the multi-material shell element in LS-DYNA, a through-thickness integration rule (in-plane integration is controlled by the shell element type) is defined. The rule specifies the number of integration layers, the distance above or below the shell mid-plane (as determined by the nodal locations) of each layer, a weighting or thickness factor for each layer, and finally which constitutive model is to be used by each layer. For the nominal RCC configuration of 19 layers, 19 integration points are used to model RCC. Two layers on both the top and bottom of the shell are allocated to the coating. Because the coating is away from the mid-plane, it is assumed that three or more integration points (to capture local bending) for each layer are not required.

Substrate

The carbon substrate is modeled with an orthotropic continuum damage mechanics model that was developed by Matzenmiller et al (11), implemented into LS-DYNA by Schweizerhof et al (12) and in order to include rudimentary strain-rate sensitivity, supplemented with a visco-elastic term which created *MAT_RATE_SENSITIVE_COMPOSITE_FABRIC (MAT 158) (10). In this constitutive model, all of the nonlinearity in the material response is assumed to be due to damage mechanisms, which does an excellent job of reproducing the nonlinear stress-strain behavior of the substrate.

MAT 158 uses an orthotropic formulation, in which the user specifies an initial elastic modulus in the in-plane directions, a Poisson's ratio coupling those two directions, and an in-plane shear modulus. These constants are obtained through static tests, and in the case of the RCC substrate the information can be found in Baccus (9). To model the nonlinear damage response, a failure stress and strain are defined which are not necessarily related to the initial elastic modulus. Given the initial modulus and this failure coordinate, the MAT 158 model computes the Weibull distribution that fits these two conditions. The model uses a variable " ω " to specify the current state of damage. As the material is damaged, ω represents the amount of material that can no longer carry load, such that the mean stress through any cross-section ($\hat{\sigma}$) is related to the stress in the undamaged material (σ) through

$$\hat{\sigma} \equiv \sigma \cdot (1 - \omega) \quad [2]$$

and it is assumed that the undamaged material obeys Hooke's law, leaving the total average response to be:

$$\frac{\hat{\sigma}}{1 - \omega} = E \cdot \varepsilon. \quad [3]$$

Coating

Because of the unusual properties of the coating (the nonlinear stress/strain response and the tension cracks) no appropriate material model existed in LS-DYNA or in the literature. A new constitutive model was created and included in LS-DYNA as MAT 236, *MAT_NON_LINEAR_ELASTIC_TENSION_CRACKS. The compression and shear coating properties can be satisfied with a simple, orthotropic, linear-elastic model. It was assumed that that the coating is not rate-sensitive.

The constitutive model for the silicon carbide coating on RCC is based upon a quasi-orthotropic, linear-elastic, plane-stress model, given by

$$\begin{Bmatrix} \sigma_1 \\ \sigma_2 \\ \tau_{12} \end{Bmatrix} = \begin{bmatrix} \frac{E}{1-\nu^2} & \frac{\nu E}{1-\nu^2} & 0 \\ \frac{\nu E}{1-\nu^2} & \frac{E}{1-\nu^2} & 0 \\ 0 & 0 & G_{12} \end{bmatrix} \begin{Bmatrix} \varepsilon_1 \\ \varepsilon_2 \\ \gamma_{12} \end{Bmatrix}. \quad [4]$$

The relatively small amount of stress that the coating can bear in tension is represented in the model by a simple, non-damage stress cutoff in tension. The stress in tension is limited to a specified value, but the behavior in compression is not affected. The tensile "yielding," modeled by the stress-cutoff, is fully recoverable as it is not plasticity or damage based. This is consistent with the physical behavior of the coating.

The tension stress-cutoff separately resets the stress to a limit value when it is exceeded in each of the two principal directions. There is also a strain-based memory criterion that ensures

unloading follows the same path as loading; the “memory criterion” is the tension stress assuming that no stress cutoffs were in effect. In this way, when the memory criterion exceeds the user-specified cutoff stress, the actual stress will be set to that value. When the element unloads and the memory criterion falls back below the stress cutoff, normal behavior resumes. Using this criterion is a simple way to ensure that unloading does not result in any hysteresis. The cutoff criterion cannot be based on an effective stress value because effective stress does not discriminate between tension and compression, and also includes shear. This means that the in plane, 1- and 2- directions must be modeled as independent to use the stress cutoff. Because the Poisson’s ratio is not zero, this assumption is not true for cracks that may arbitrarily lie along any direction. However, careful examination of damaged RCC shows that generally, the surface cracks do tend to lie in the fabric directions as seen in Figure 9, meaning that cracks tend to open in the 1- or the 2- direction independently. So the assumption of directional independence for tension cracks may be appropriate for the coating because of this observed orthotropy.

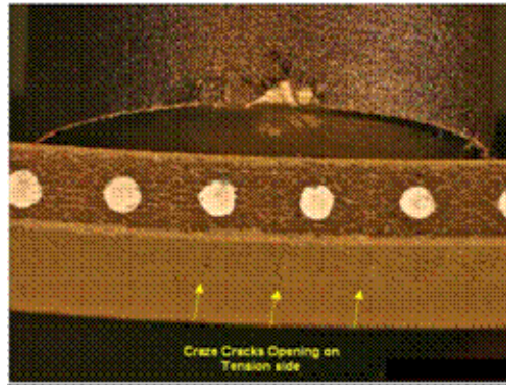


Figure 9. An RCC specimen in bending, with “craze cracks” opening on the tension side.

The quasi-orthotropic, linear-elastic, plane-stress model with tension stress cutoff (to simulate tension cracks) can model the linear coating properties, but cannot model nonlinear response. A nonlinear-elastic stress-strain relationship can also be modeled using MAT 236. Thus, instead of $\underline{\sigma} = \mathbf{E} \cdot \underline{\varepsilon}$, the modulus will be defined as a function of some effective strain quantity, or $\underline{\sigma} = \mathbf{E}(\varepsilon_{eff}) \cdot \underline{\varepsilon}$.

The von Mises strain is selected for the effective strain definition as it couples the 3-dimensional loading but reduces to uniaxial data, so that the desired uniaxial compressive response can be reproduced. So,

$$\varepsilon_{eff} = \frac{1}{\sqrt{2}} \frac{1}{1+\nu} \sqrt{(\varepsilon_1 - \varepsilon_2)^2 + (\varepsilon_2 - \varepsilon_3)^2 + (\varepsilon_1 - \varepsilon_3)^2 + 3\gamma_{12}^2} \quad [5]$$

where for a 2-D, isotropic shell element case, the z-direction strain is given by

$$\varepsilon_3 = \frac{-\nu}{1-\nu} (\varepsilon_1 + \varepsilon_2). \quad [6]$$

The function for modulus is implemented as an arbitrary 5th order polynomial

$$E(\varepsilon_{eff}) = A_0 \cdot \varepsilon_{eff}^0 + A_1 \cdot \varepsilon_{eff}^1 + \dots + A_5 \cdot \varepsilon_{eff}^5. \quad [7]$$

In the case of linear material the first coefficient (A_0) is simply the modulus E , and the other coefficients ($A_{n>0}$) are zero, reducing to a 0th order polynomial.

For values of strain which exceed the failure strain observed in the laminate compression tests, the higher order polynomial will no longer match the test data. Therefore, after a specified effective-strain, representing failure, the modulus is defined to be the tangent of the polynomial curve. As a result, the stress/strain response has a continuous derivative, which aids in avoiding numerical instabilities.

The two dominant modes of loading which cause coating loss on the impact side of the RCC (the front-side) are in-plane compression and transverse shear. The in-plane compression is measured by the peak out of plane tensile strain, ε_3 . As there is no direct loading of a shell element in this direction, ε_3 is computed through Poisson's relation, as given in equation [6]. When ε_3 is tensile, it implies that the average of ε_1 and ε_2 is compressive. This failure mode will likely dominate when the RCC undergoes large bending, putting the front-side coating in high compressive strains.

The transverse shear failure mode will dominate when the debris source is very hard or very fast. By definition, the shell element cannot give a precise account of the transverse shear throughout the RCC's thickness. The Belytschko-Tsay shell element formulation in LS-DYNA has a first-order approximation of transverse shear (13) that is based on the out-of-plane nodal displacements (w) and rotations (θ) that should suffice to give a qualitative evaluation of the transverse shear,

$$\begin{aligned} 2\varepsilon_{xz} &= \frac{\partial w}{\partial x} + \theta_y \\ 2\varepsilon_{yz} &= \frac{\partial w}{\partial y} - \theta_x \end{aligned} \quad [8]$$

By this formulation, the transverse shear is constant through the entire shell thickness and thus violates surface-traction conditions. The constitutive model implementation records the peak value of the tensile out-of-plane strain (ε_3) and peak root-mean-sum transverse-shear, $\sqrt{\varepsilon_{13}^2 + \varepsilon_{23}^2}$. In addition, the model calculates the thru-thickness principle strain at the substrate-coating interface layer by combining the in-plane strain, the out-of-plane strain (as in equation [6]), and the transverse shear (as in equation [8]). These values can then used to correlate the analytical predictions to the ballistic test results, and will be discussed in the next section.

Results

The analytical model is compared to three tiers of testing; material coupon tests (9,14-16), controlled flat RCC panel impact tests (3,17), and finally impact testing of a full Orbiter panel (4). The end result of the RCC model is its use to predict the damage seen in the full panel configuration, but it must first be verified by reproducing laminate and constituent (substrate and coating) stress/strain curves, bending load vs. deflection, flat panel deflections, and full panel deflections.

Static Test Comparisons

Figure 10 presents the average tension response of the substrate, laminate, and coating compared to the model predictions (dashed lines). The substrate model predicts the initial modulus and failure point exactly, as these are model inputs, but MAT 158 does not exactly match the full substrate response. The stress limit of about 1/3 of the computed failure stress was specified as an approximation of the coating response. Clearly this is not a perfect match, but since the substrate dominates in tension, the overall effect of the coating's tension properties is small. Combining the substrate and coating models into the laminate prediction produces a fairly good match to the average laminate test data.

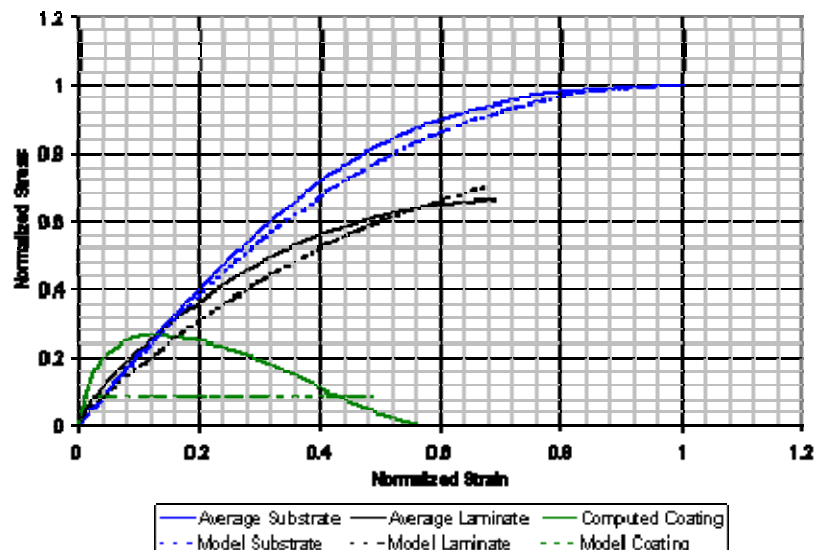


Figure 10. Comparison of coating, substrate, and laminate model to material properties in tension.

Figure 11 shows the compression response of the substrate, coating, and laminate. In this case, the substrate response is very precisely modeled by the Weibull distribution, and the coating model precisely matches the linear coating response. The two combine to precisely match the laminate test data, as expected.

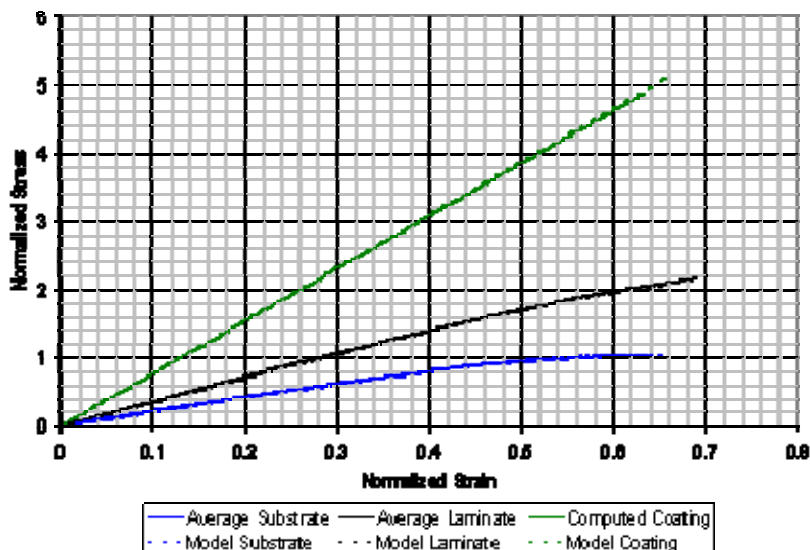


Figure 11. Comparison of coating, substrate, and laminate model to material properties in compression.

Figure 12 shows the in-plane shear comparison. According to Baccus (10), only two laminate material tests yielded good strain data. The nonlinear coating response is computed from these two tests and the substrate average is ignored. In the model, the coating is assumed to be linear in shear. That this is a good approximation for the first part of loading is demonstrated by Figure 12.

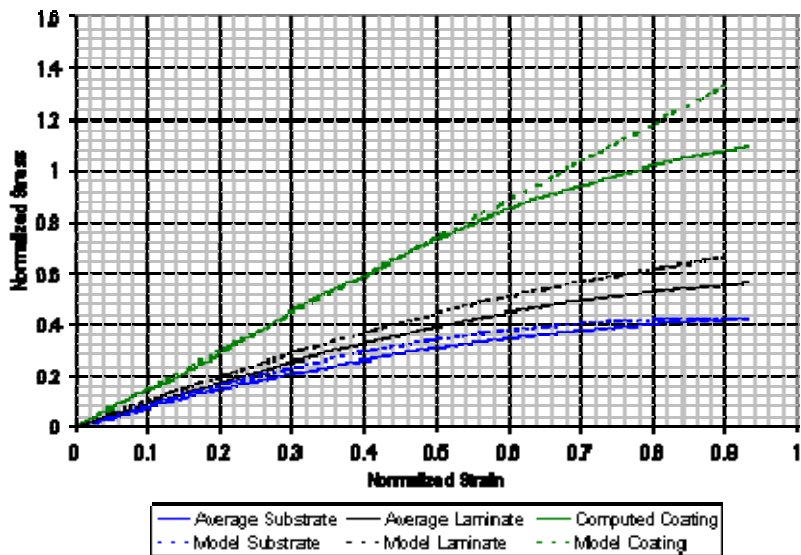


Figure 12 Comparison of coating, substrate, and laminate model to material properties in in-plane shear.

3-Point Bending Test Comparison

3-point bend tests were performed at NASA’s Langley Research Center by Fasanella, Kellas, et al (18). As shown in Figure 13, the force vs. deflection curves of the test and analysis matched very well.

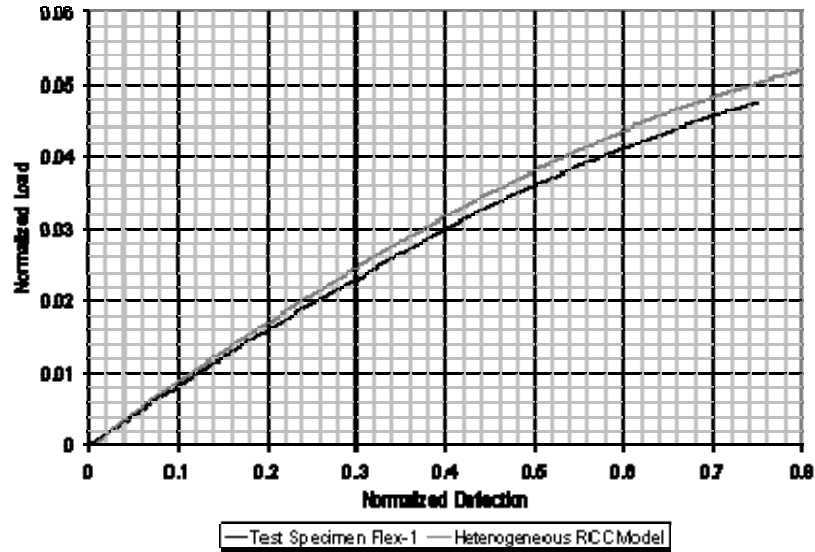


Figure 13. Comparison of RCC model to as-fabricated RCC bend test.

High Strain Rate Material Property Tests

High strain rate testing was performed by Gilat (16). Figure 14 demonstrates that the substrate-only high rate comparisons show good agreement. Figure 15 shows the laminate tension response at a high strain rate (270 1/s). Note the scatter in the test data, and that the laminate response matches appropriately, confirming the modeling approximation that only the substrate shows strain-rate effects.

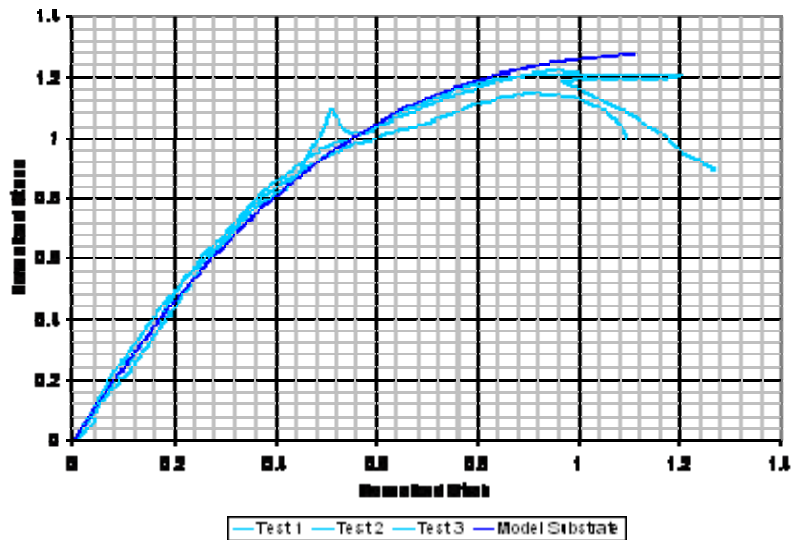


Figure 14. RCC Substrate test data in high-rate ($2.5-2.7 \times 10^2 \text{ s}^{-1}$) tension, with substrate model.

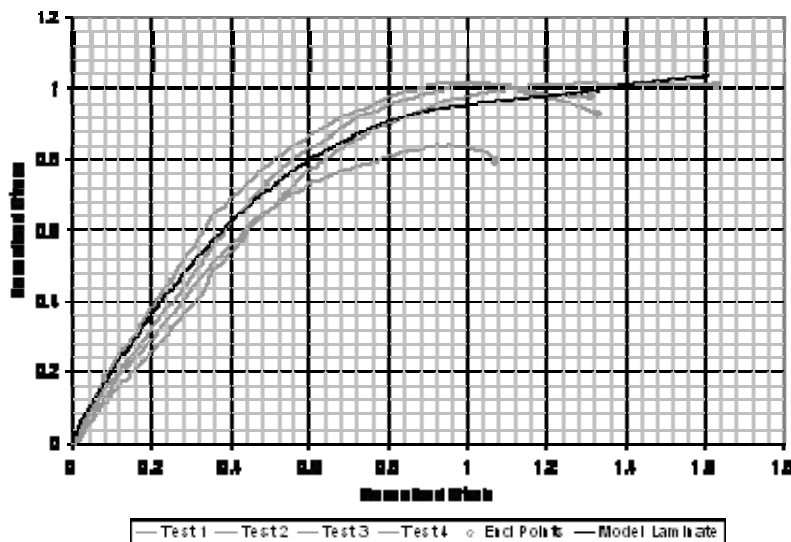


Figure 15. Laminate test data in high-rate ($2.7 \times 10^2 \text{ s}^{-1}$) tension, with RCC model comparison.

Verification Impact Tests – Deflections

A series of debris impact tests were performed to verify the constitutive models and finite element models which have been developed (3,4,17). Three panel types were used in the impact analyses: 6" by 6" flat panels, 6" by 12" flat panels, and full-scale panels. Because strain-based failure criteria are mesh size sensitive, a element edge length of 0.1" was chosen to accommodate all panel sizes. Nodal displacements were used as a convergence check, and for the debris sizes used in these impact tests, this discretization was adequate.

The debris sources used as projectiles in these impacts were BX-265 and PDL external tank foam and ice. The foam models are parameterized by using static and high-rate compression and standard LS-DYNA standard models (7). The ice model is a phenomenological model that undergoes a transformation from an elastic solid to a hydrostatic fluid when a failure criterion is met. A more complete description of the Eulerian ice formulation can be found in (19).

Figure 16 shows the displacement time-history for 5 locations in a 6"x6" flat panel, impacted by an ice cylinder: the center of the panel (the impact location), and 4 points one-inch away from center. The agreement is excellent with both the peak displacements and the response frequency being captured.

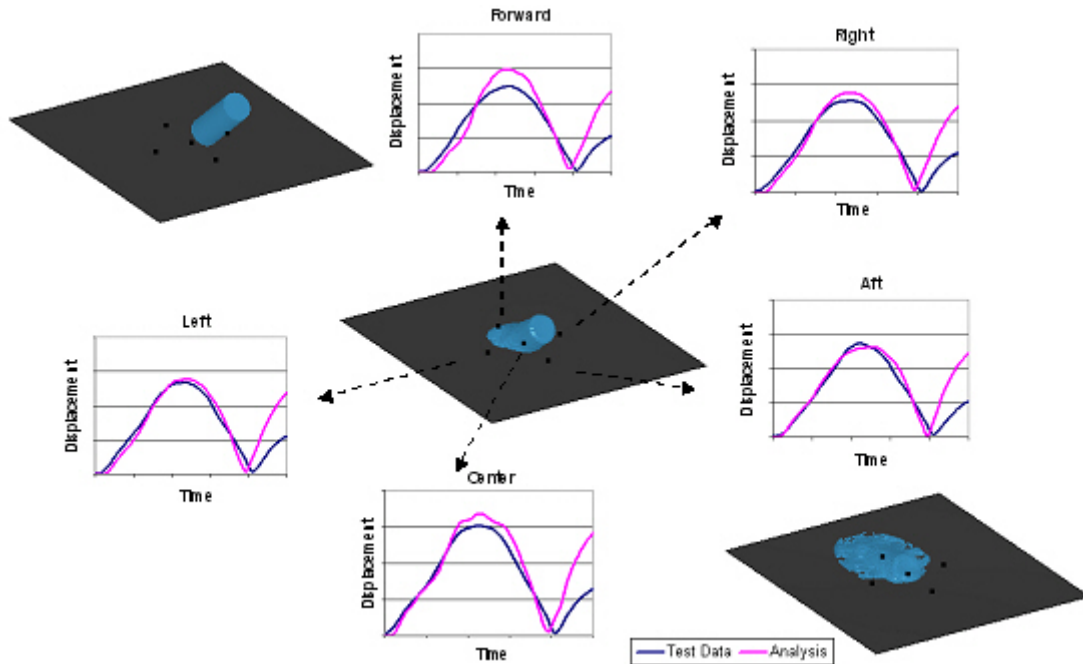


Figure 16. Deflection comparisons at 5 panel locations during a typical 45° ice impact on a 6''x6'' RCC flat plate.

Next, Figures 17 and 18 show comparisons of the center displacement on 6''x12'' flat plates. Figure 17 shows another ice impact and Figure 18 shows a BX-265 foam impact. Again, the agreement is excellent considering test uncertainties and RCC material property scatter, and so there is good confidence that the RCC material model is simultaneously capturing the tension, compression, shear, bending, and high-rate properties of both the coating and the substrate.

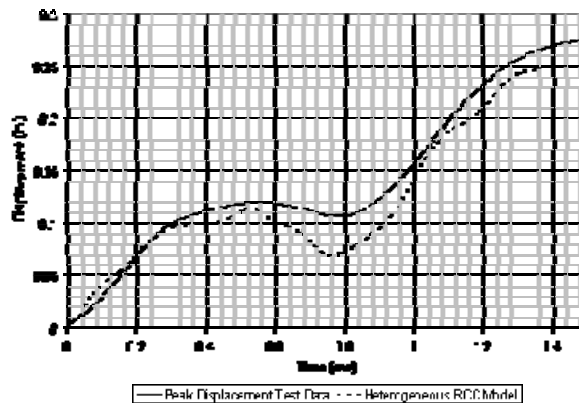


Figure 17. Center deflection of a 6''x12'' flat plate during an ice impact.

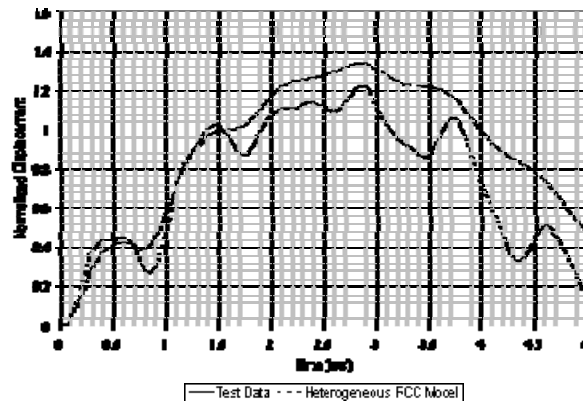


Figure 18. Center deflection of a 6''x12'' flat plate during a BX-265 foam impact.

Verification Impact Tests – Damage

The RCC constitutive model is used to determine the threshold velocity for critical damage at a particular location from a particular debris source. Dozens, hundreds, or even thousands of individual LS-DYNA analyses are performed to develop a damage threshold map defining the threshold velocities for different debris sources and masses at all RCC locations. The damage threshold map is combined with debris transport analysis (DTA) that predicts how often a debris source will impact each location and at what speed, and a probabilistic assessment (20) is done to determine the risk to the Orbiter from ascent debris sources.

Several mechanisms causing RCC critical damage have been observed (7,8,9). The two major classifications are “visible” and “non-visible” damage. The primary non-visible failure mode is a substrate delamination which can be detected using sensitive ultrasonic or pulse-thermography non-destructive evaluation (NDE) techniques. These delaminations have been shown in thermal tests to allow fast oxidation of the delaminated area, and are thus not desirable (21). Visible damages include front-side coating loss, back-side coating loss, through-thickness cracking of the substrate, and holes thru the RCC. Depending on the thermal environment at the damaged location, all or none of these types of damages may cause mission failure. Substrate delaminations and front-side coating loss are the most general types of critical damage, and will be our focus.

The ability to predict NDE-detectable damage is somewhat limited by the shell element approximation. Since the thru-thickness properties are not included, and strain/displacement continuity cannot be released in the current shell element implementation, the model cannot explicitly model delaminations. However, analysis of damaged RCC specimens indicates that damage at the lowest velocities are often fiber and matrix cracking on the side opposite the impact, which relate to the in-plane tensile failure strains of the material. Analysis of impacts near the onset of NDE-detectable damage demonstrates that this type of damage can be predicted by watching for one layer of substrate to exceed the test-average substrate failure strain. Figure 19 plots the analysis predictions for maximum strain in the innermost substrate layer for all of the RCC impact test thresholds. Using the principle thru-thickness strain improves the correlation for the hard projectile cases a small amount because of the inclusion of the transverse shear. From these analysis predictions of peak strain, a mean and standard deviation value for onset of NDE damage can be easily determined.

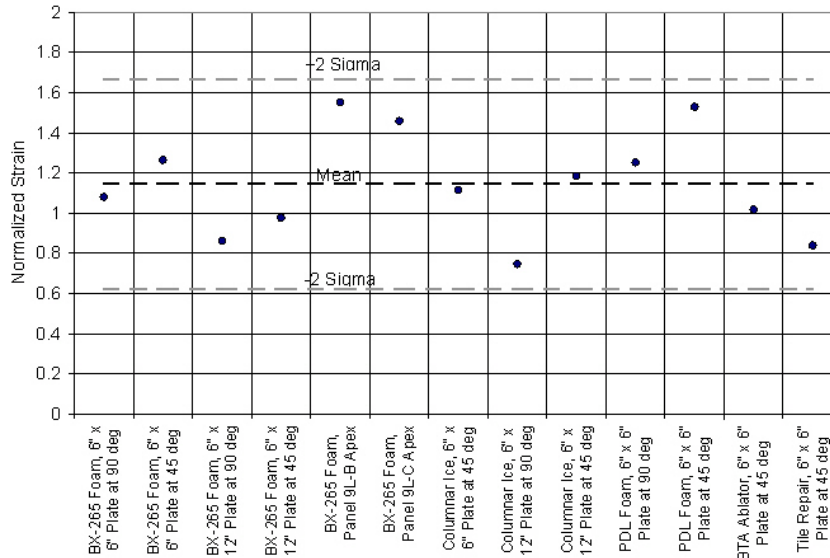


Figure 19. RCC model predictions for normalized strain at NDE damage thresholds.

In Figures 20 and 21, material tension test results are plotted along with the model’s response, and the mean and two standard deviations of strain at the onset of NDE damage are shown. The two standard deviations compare very closely with the largest and smallest failure strains for RCC. This indicates that with minor statistical variation, the RCC model predicts NDE-detectable damage onset when one substrate layer (out of a total of 15) exceeds the substrate’s failure strain, as determined through material property tests.

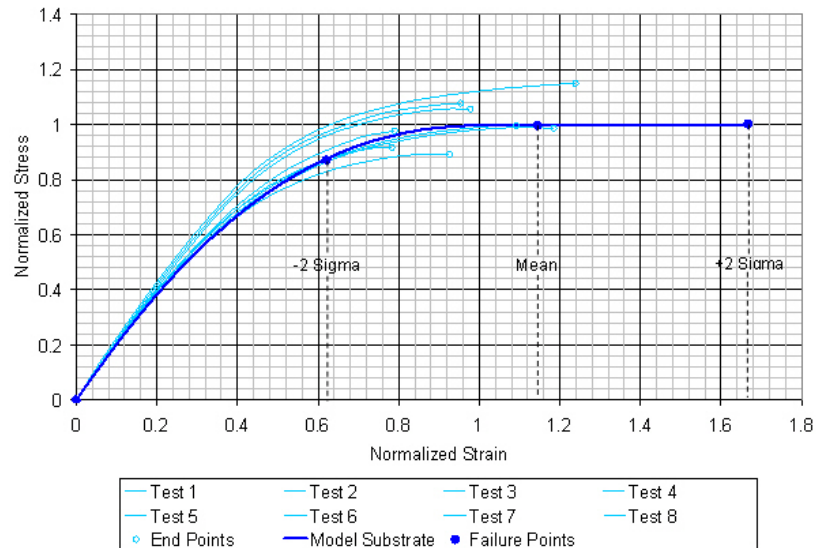


Figure 20. Substrate static tension tests plotted alongside the substrate constitutive model prediction with correlated test failure strains ($\pm 2\sigma$, mean or V50).

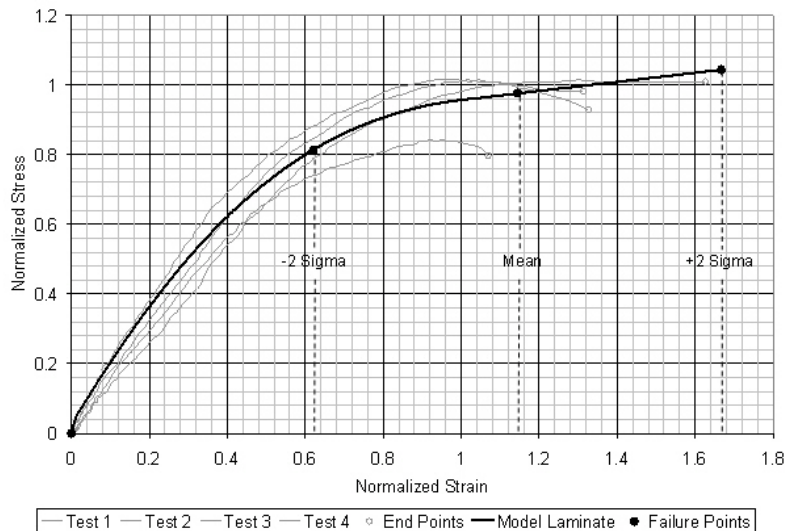
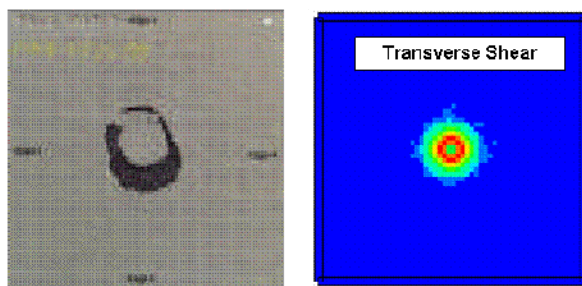
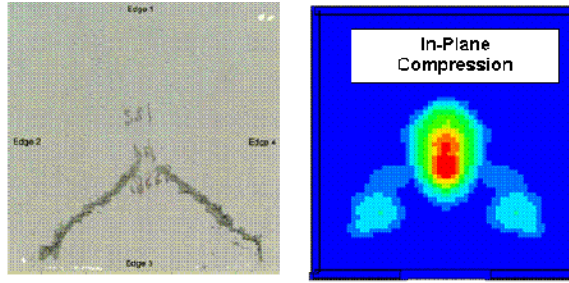


Figure 21. Laminate high-rate tension tests plotted alongside the heterogeneous constitutive model prediction, with correlated test failure strains ($\pm 2\sigma$, mean or V50).

Front-side coating damage predictions are more complex because different damage mechanisms can exist; “crushing” of the coating in compression, and “plugging,” a failure mode heavily influenced by transverse shear, appear to be the two dominant modes. Examples of each failure mode are seen in the 6”x6” RCC plate impacts; ice impacting at 90°, resulting in plugging failure, is dominated by transverse shear, and foam impacting at 45°, resulting in crushing failure, is dominated by in-plane compression. Figure 22 shows the plugging damage resulting from the ice impact and the maximum transverse shear from the analysis. The maximum transverse shear is highest along the edge of the projectile as is the observed failure. Figure 23 shows the crushing damage resulting from the foam impact, along with the peak ϵ_3 from the analysis, representing the amount of in-plane compression. The in-plane compression is high along the same V-shape pattern as the observed failure, and transverse shear levels are low compared to the ice impact, and not in the V-shape pattern, indicating that there are two different modes of failure in these two examples.



Analysis shows qualitatively high levels of transverse shear in the same pattern.
 Figure 22. Ice impact resulting in a ring of lost coating, outlining the impact area.



Analysis shows high levels of in-plane compression in the same V-shaped pattern, indicating that this is the dominant failure mode. Transverse shear levels are low compared to Figure 22.

Figure 23. Foam impact resulting in a V-shaped pattern of crushed coating.

The model’s damage predictions are correlated to both kinds of front-side damage: plugging and crushing. Because many impacts are dominated by one or the other, they will be considered separately when possible. In the same manner as NDE damage, the analysis predictions for peak transverse shear or peak ϵ_3 are plotted for each front-side damage threshold in Figure 24. The means and two standard deviations are plotted as well.

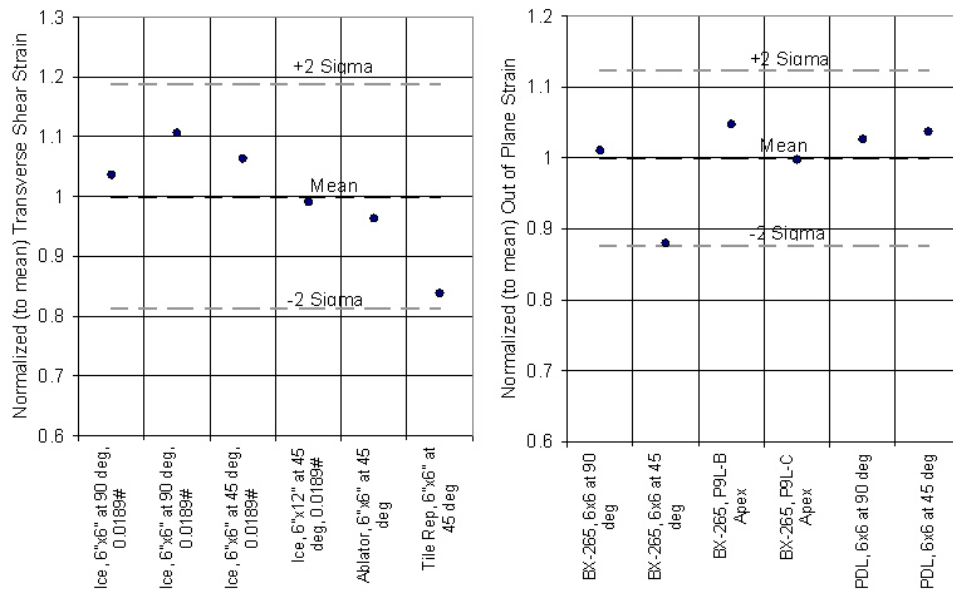


Figure 24. RCC model predictions for peak transverse shear and peak ϵ_3 at front-side coating loss thresholds.

The in-plane compression failure, as determined through ϵ_3 , can be compared to RCC compression tests. Equation [6] can be re-written to give the average in-plane compression strain,

$$\frac{\epsilon_1 + \epsilon_2}{2} = \frac{1}{2} \frac{(\nu - 1)}{\nu} \epsilon_3 \tag{9}$$

For front-side coating compressive failure, the onset of failure occurs when the average in-plane compressive strain reaches the average RCC laminate compressive failure strain. This value is difficult to obtain by testing and so the coating model compressive failure criterion does not match a material property, but it does show consistency with the RCC laminate compression tests.

The transverse-shear damage criterion from the model also can not be related to a material property because the shell element utilizes the first-order transverse shear theory, as in equation [8], and this does not accurately capture the transverse shear strains through the thickness of the RCC. It does, however, give a reasonable, qualitative estimate of average transverse shear magnitude. This value has been empirically correlated to the impact test data and used to predict plugging failures.

Conclusions

A heterogeneous formulation for RCC has been presented, which improves on the previous RCC approximate model, producing accurate modeling of deflections during an impact event. In order for the heterogeneous model to predict the proper deflections of RCC during an impact event, it was necessary to create a new constitutive model for the coating. This model does not attempt to capture the micro-scale physics of the coating, nor its damage mechanisms, as it makes the approximation of nonlinear elasticity to capture the proper stress/strain response. The coating and RCC laminate models capture the desired macroscopic stress/strain responses, as seen in the accurate matching of material test data, as well as full-field impact displacement data. As a consequence of the accurate representation of deflection and stress within the entire RCC laminate, the onset of NDE-detectable damage matched the static strain-to-failure data, a basic physical property, giving confidence in the important transition from as-fabricated to flight-degraded material modeling, where impact tests are few. Additionally, coating in-plane compressive strain and first-order transverse shear strain was correlated to front-side coating damage for as-fabricated material.

References

1. M. Gordon, "Leading Edge Structural Subsystem and Reinforced Carbon-Carbon Reference Manual," Boeing Report KL0-98-088, October 1998.
2. H. Gehman, et al, "Columbia Accident Investigation Board Report." U.S. Government Printing Office, August 2003.
3. M. Melis, M. Pereira, D. Revilock, K. Carney, "A Summary of the NASA Glenn Ballistic Impact Lab Contributions to the Columbia Accident Investigation and NASA's Return-to-Flight Effort", Annual Reliability and Maintainability Symposium, 2005.
4. D. Grosch and F. Bertrand, "Thermal Protection System (TPS) Impact Experiments." 47th AIAA/ASME/ASCE/AHS/ASC Structures, Structural Dynamics and Materials Conference, 2006.
5. Livermore Software Technology Corporation, P.O. Box 712, Livermore, CA 94551-0712.
6. M. Melis, K. Carney, J. Gabrys, E. Fasanella, K. Lyle," A Summary of the Space Shuttle Columbia Tragedy and the Use of LS-DYNA in the Accident Investigation and Return to Flight Efforts." 8th International LS-DYNA User's Conference, 2004.
7. K. Carney, M. Melis, E. Fasanella, K. Lyle, J. Gabrys, "Material Modeling of Space Shuttle Leading Edge and External Tank Materials For Use in the Columbia Accident Investigation.," 8th International LS-DYNA User's Conference, 2004.
8. T.W. Smith, et al, "Leading Edge Structural Subsystem Mechanical Design Allowables for Material with Improved Coating System," *LORAL Vought Systems* Report No. 221RP00614, Revision A, October 1994.
9. R.K. Baccus, "Mechanical Property Characterization of Reinforced Carbon-Carbon for the Space Shuttle Return-to-Flight Effort." NASA TM JSC-63036, 2006.
10. Livermore Software Technology Corporation (LSTC). "LS-DYNA Keyword User's Manual." Version 971, Livermore, CA, May 2007.
11. Matzenmiller, Lubliner, and Taylor, Mechanics of Materials, 20, 1995.
12. K. Schweizerhof, K. Weimar, Th. Munz, Th. Rottner, LS-DYNA World Conference, 1998.
13. R. Tanov, A. Tabiei, 6th International LS-DYNA User's Conference, 2000.

14. J. Koenig, "RCC Carbon-Carbon Material Characterization." Southern Research Institute Report No. SRI-ENG-03-41-A359.14, 2003.
15. J. Koenig, "Uncoated RCC Material Characterization." Southern Research Institute Report No. SRI-ENG-05-41-A359.14, 2005.
16. A. Gilat, "Tensile Testing of RCC at Various Strain Rates." Ohio State University, RF Project No. 746182, 2005.
17. M. Melis, D. Revilock, J. Pereira, K. Lyle, "Impact Testing on Reinforced Carbon-Carbon Flat Panels With BX-25 and PDL-1034 External Tank Foam for the Space Shuttle Return to Flight Program." NASA TM-213642, 2007.
18. E. Fasanella and S. Kellas, "Quasi-Static 3-Point RCC Bend Test and Analysis for Shuttle Orbiter Wing Leading Edge Impact Damage Thresholds." NASA TM-214505, 2006.
19. K. Carney, P. DuBois, D. Benson, R. Lee, International Journal of Solids and Structures, **43**, 2006.
20. L. Huyse, B. Thacker, D. Riha, S. Fitch, J. Pepin, E. Rodriguez, 47th AIAA/ASME/ASCE/AHS/ASC Structures, Structural Dynamics and Materials Conference, 2006.
21. T. Horvath, 42nd AIAA Aerospace Sciences Meeting, 2004.

